

# Raman spectroscopic study of the effect of the use of laser/LED phototherapy on the repair of complete tibial fracture treated with internal rigid fixation

Antônio L.B. Pinheiro<sup>1,2,\*</sup>, Luiz G.P. Soares<sup>1,2</sup>, Aline C.P. da Silva<sup>1</sup>, Nicole R.S. Santos<sup>1</sup>, Anna Paula L.T. da Silva<sup>1</sup>, Bruno Luiz R.C. Neves<sup>1</sup>, Amanda P. Soares<sup>1</sup>, Landulfo Silveira Jr.<sup>3</sup>

<sup>1</sup> Center of Biophotonics, School of Dentistry, Federal University of Bahia – UFBA, Av. Araújo Pinho, 62, Canela, Salvador, BA, 40110-150, Brazil

<sup>2</sup> National Institute of Basic Optics and Applied to Life Sciences, Physics Institute of São Carlos, University of São Paulo – USP, Av. Trabalhador São-Carlense, 400, Parque Arnold Schmidt, São Carlos, SP, 13566-590, Brazil

<sup>3</sup> Center for Innovation, Technology and Education – CITE, Universidade Anhembi Morumbi – UAM, Parque Tecnológico de São José dos Campos, Estr. Dr. Altino Bondensan, 500, Eugênio de Melo, São José dos Campos, SP, 12247-016, Brazil

## ARTICLE INFO

### Keywords:

Raman spectroscopy  
light phototherapy  
internal rigid fixation  
mineral trioxide aggregate (MTA)  
bone repair

## ABSTRACT

This study aimed to assess the repair of complete surgical tibial fractures fixed with internal rigid fixation (IRF) associated or not to the use of mineral trioxide aggregate (MTA) cement and treated or not with laser ( $\lambda = 780$  nm, infrared) or LED ( $\lambda = 850 \pm 10$  nm, infrared) lights,  $142.8 \text{ J/cm}^2$  per treatment, by means of Raman spectroscopy. Open surgical tibial fractures were created on 18 rabbits (6 groups of 3 animals per group, ~8 months old) and fractures were fixed with IRF. Three groups were grafted with MTA. The groups of IRF and IRF + MTA that received laser or LED were irradiated every other day during 15 days. Animals were sacrificed after 30 days, being the tibia surgically removed. Raman spectra were collected via the probe at the defect site in five points, resulting in 15 spectra per group (90 spectra in the dataset). Spectra were collected at the same day to avoid changes in laser power and experimental setup. The ANOVA general linear model showed that the laser irradiation of tibial bone fractures fixed with IRF and grafted with MTA had significant influence in the content of phosphate (peak  $\sim 960 \text{ cm}^{-1}$ ) and carbonated (peak  $\sim 1,070 \text{ cm}^{-1}$ ) hydroxyapatites as well as collagen (peak  $1,452 \text{ cm}^{-1}$ ). Also, peaks of calcium carbonate ( $1,088 \text{ cm}^{-1}$ ) were found in the groups grafted with MTA. Based on the Raman spectroscopic data collected in this study, MTA has been shown to improve the repair of complete tibial fractures treated with IRF, with an evident increase of collagen matrix synthesis, and development of a scaffold of hydroxyapatite-like calcium carbonate with subsequent deposition of phosphate hydroxyapatite.

## 1. Introduction

Rigidity, elasticity and firmness are characteristics of bone tissue derived its matrix and are closely related to the formation process of the crystalline solid apatite as well as by the flow and availability of individual constituents such as calcium. Pathologies, trauma, or surgical procedures may cause bone losses. Large bone defects often demand the use of grafts including the use of biomaterials as the bone may not be able to repair itself. Several techniques have been proposed for the treatment of bone defects, including the use of several types of grafts, membranes, and the association of both techniques [1,2].

Fractures are very common lesions worldwide. Although their treatment has advanced along the time, 5%-10% of fractures still show

delayed union or nonunion [3]. Fractures have been treated with immobilization, traction, amputation, and internal fixation. The choice of the type of internal fixation depends on the type of fracture, the condition of the soft tissues and bone, the size and position of the bone fragments, and the size of the bony defect [4,5]. Internal rigid fixation (IRF) is used in the treatment of fractures as it provides sufficient stability for fracture repair using miniplates.

Over the past years, the cellular activity during bone repair has been stimulated by several methods including the use of several types of energy emitters such as ultrasound, electrical stimulation, laser and LED lights [6–13]. Light phototherapy is an interesting therapeutic approach and various experimental studies have demonstrated beneficial effects of the use of laser light on bone metabolism and fracture

\* Corresponding author at: Center of Biophotonics, School of Dentistry, Federal University of Bahia – UFBA, Av. Araújo Pinho, 62, Canela, Salvador, BA, 40110-150, Brazil.

E-mail address: [albp@ufba.br](mailto:albp@ufba.br) (A.L.B. Pinheiro).

<https://doi.org/10.1016/j.pdpdt.2020.101773>

Received 18 September 2019; Received in revised form 17 March 2020; Accepted 2 April 2020

Available online 18 April 2020

1572-1000/ © 2020 Elsevier B.V. All rights reserved.

consolidation [10–16]. However, the protocols proposed so far have not been enough for a full determination of optimal parameters. The wide range of possible combinations of the laser parameters made very complex the establishment of an effective protocol [1].

The light irradiation of tissues possesses a wavelength dependent capacity of altering the cellular behavior in the absence of significant heating. The dispersion of the light in the tissue is a complex process as tissues components influence the dispersion. Studies indicate that bone irradiated mostly with IR wavelengths shows increased osteoblastic proliferation, collagen deposition and bone neof ormation when compared to non-irradiated bone [17]. It is known that the stimulant effect of the light on bone occurs during the initial phase of proliferation of both fibroblasts and osteoblasts as well as on initial differentiation of mesenchymal cells. Fibroblastic proliferation and its increased activity have been detected previously on irradiated subjects and cells cultures and these are responsible for great concentration of collagen fibers seen within irradiate bone [1]. Our group have used Raman spectroscopy as a method for assessment of the effects of phototherapies on the repair process of fractures using different animal models [1,4,5,14–16].

Autologous bone grafts or biomaterials are often used as therapeutic strategies to fill the bone defects for reconstructing large bone defects. A good bone graft-substitute needs to be biocompatible, bioresorbable, osteoconductive, osteoinductive, structurally like bone, and easy or ready to use [18–20]. Different biomaterials of both animal or human and synthetic origin have been extensively studied [1,4,5,14–20] as filling materials. Mineral trioxide aggregate (MTA) is a powder aggregate containing mineral oxides that presents good biological response without cytotoxicity [21] and stimulates tissue repair by increasing cellular adhesion, growth, and proliferation, the deposition of new bone, and induces spontaneous formation of a calcium phosphate layer when immersed in physiological fluids [22–31]. This bone-like apatite layer supports new tissue formation, and its integration in the bone tissue represents an essential requirement for an artificial material to be considered osteoconductive and osteoinductive [22–31]. MTA is indicated when moisture control is inadequate, without loss of its properties, and it is not reabsorbable [32,33]. Additionally, MTA has antibacterial properties [29]; enhanced tissue dissolution; and induces bone formation [30]. It has been suggested that a rise in pH induced by calcium hydroxide combined with the availability of  $\text{Ca}^{2+}$  and  $\text{OH}^-$  ions causes stimulation of the enzymatic pathways and, therefore, bone mineralization [34].

Raman spectroscopy has been used for qualitative and quantitative evaluation of the biochemical composition of biological tissues and fluids as well as for monitoring biological processes non-destructively [35–38]. Changes in the shape, position, intensity and/or area of the most relevant peaks in Raman spectra are suggestive of changes in the metabolism and differences in the structural conformations of biomolecules [35,37]. The Raman spectrum of bone shows prominent vibrational bands related to tissue composition. Raman bands with peaks at  $\sim 960$ ,  $\sim 1,045$  and  $\sim 1,070 \text{ cm}^{-1}$  are attributed to calcium hydroxyapatite (both phosphate and carbonated, respectively), and the bands with peaks at  $\sim 1,452$  and  $\sim 1,660 \text{ cm}^{-1}$  are attributed to collagen from the matrix [39,40]. Raman spectroscopy could be a method to assay bone mineralization and remodeling by evaluating the changes in the Raman bands, *in situ* and rapidly, without sample preparation or tissue destruction [39,40].

Recent studies showed that the use of grafting biomaterial MTA in association with (LED and laser) phototherapy could improve the repair of complete tibial fractures on an animal model [1,4,5,14–16]. Therefore, the aim of this study was to evaluate the repair of complete tibial fractures that have been treated with internal rigid fixation (IRF) by miniplates associated or not with the use of MTA and laser or LED phototherapy ( $\lambda = 780 \text{ nm}$  and  $\lambda = 850 \pm 10 \text{ nm}$ , respectively, applied every other day during 15 days) after 30 days of treatment using the intensities of the Raman peaks of phosphate and carbonated HA ( $\sim 960$  and  $\sim 1,070 \text{ cm}^{-1}$ , respectively) and collagen ( $\sim 1,452 \text{ cm}^{-1}$ ) as

**Table 1**

Description and distribution of the experimental groups, with the method of bone fixation, use of MTA, and type of irradiation.

| Group             | Number of animals | Fixation method | MTA | Irradiation |
|-------------------|-------------------|-----------------|-----|-------------|
| IRF               | 3                 | Miniplate       | No  | No          |
| IRF + Laser       | 3                 | Miniplate       | No  | laser       |
| IRF + LED         | 3                 | Miniplate       | No  | LED         |
| IRF + MTA         | 3                 | Miniplate       | Yes | No          |
| IRF + MTA + Laser | 3                 | Miniplate       | Yes | laser       |
| IRF + MTA + LED   | 3                 | Miniplate       | Yes | LED         |

markers of the remodeling/repair process.

## 2. Materials and methods

### 2.1. Sampling

The study has been approved by the Animal Ethics Committee of the School of Dentistry of the Federal University of Bahia (Protocol 17/10/2012) following the same irradiation protocol (laser and LED wavelengths, energy density per lesion and time intervals) as described in previous studies [41] and commonly employed in similar light irradiation protocols [4,5,14–16]. In the present study, eighteen healthy adult male New Zealand rabbits ( $\sim 8$  months old, mean weight 2 kg) were kept during the experimental period. These animals were maintained in individual metallic cages, maintained at 12-h day/night light cycle, with controlled temperature ( $25^\circ\text{C}$ ) and humidity (60%), being fed with standard laboratory pelleted food and water *ad libitum* during the experimental period. The animals were randomly distributed into six groups (Table 1). The number of animals per group was estimated using the formula presented in Cochran (1967) [42] for finite population studies, where the parameters were defined as: confidence level of 95%, alpha level (type I error) of 5% ( $p$  - value), power of the test of 80% and an expected difference between the groups of 1.2 (already identified in previous studies [43–45], being the resulting number of animals to be 3).

### 2.2. Surgical procedure

The animals were anesthetized for the surgical procedure. For initial sedation, it was administered acepromazine (Acepran® 0.2%, 2 mg/kg; Univet S.A., Cambuci, SP, Brazil). Then general anesthesia was carried out 20 min later with ketamine (Ketalar® 50 mg/mL, 0.4 mL/kg; Lab. Parke Davis Ltda., São Paulo, SP, Brazil) and xylazine (Rompum® 20 mg/mL, 0.2 mL/kg; Bayer Health Care S.A., São Paulo, SP, Brazil). After 30 min, the right leg was shaved, and an incision 3 cm-long was performed at the right tibia with a no. 15 scalpel blade. The bone was exposed after dissection of the skin and subcutaneous tissues down to the periosteum. Finally, a complete fracture was created on the animals' tibia (transverse osteotomy at mid-point of the tibia diaphysis) with a carborundum disk (Moyco Technologies, Inc., York, PA, USA) under water refrigeration. The size of the defect was that of the thickness of the disk ( $\sim 0.5 \text{ mm}$ ).

### 2.3. Internal rigid fixation and laser/LED irradiation

Animals in group IRF had the bone fragments fixed with miniplates (MDT, Indústria Comércio Importação e Exportação de Implantes Ltda., Rio Claro, SP, Brazil) (Fig.1A), and animals in groups MTA were grafted with the biomaterial MTA (MTA Angelus®, Angelus Indústria de Produtos Odontológicos S.A., Londrina, PR, Brazil) prior similar fixation with miniplates used on group IRF. Animals in groups IRF + MTA + Laser and IRF + MTA + LED were further irradiated with laser light [Twin Flex Evolution®, MM Optics Ltda., São Carlos, SP, Brazil,  $\lambda = 780 \text{ nm}$ , 70 mW continuum, spot area  $0.5 \text{ cm}^2$ ,  $20.4 \text{ J/cm}^2$

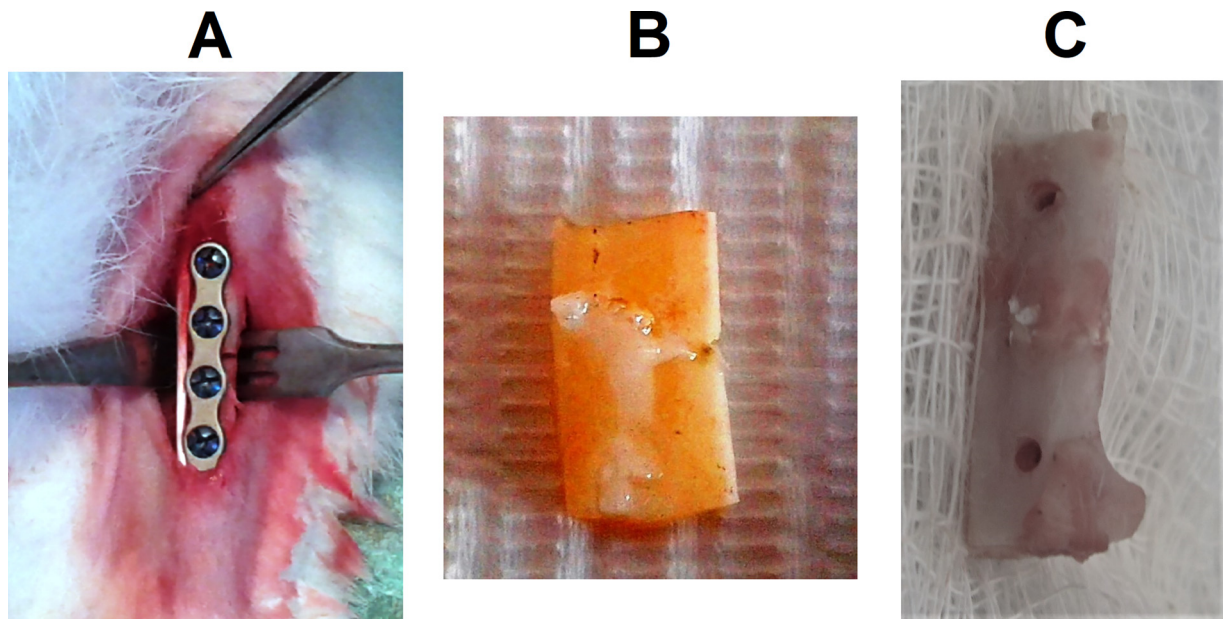


Fig. 1. A) Surgical field showing the fracture filled with MTA and the fixation with miniplate. B) Bone sample showing the defect site 30 days after fracture.

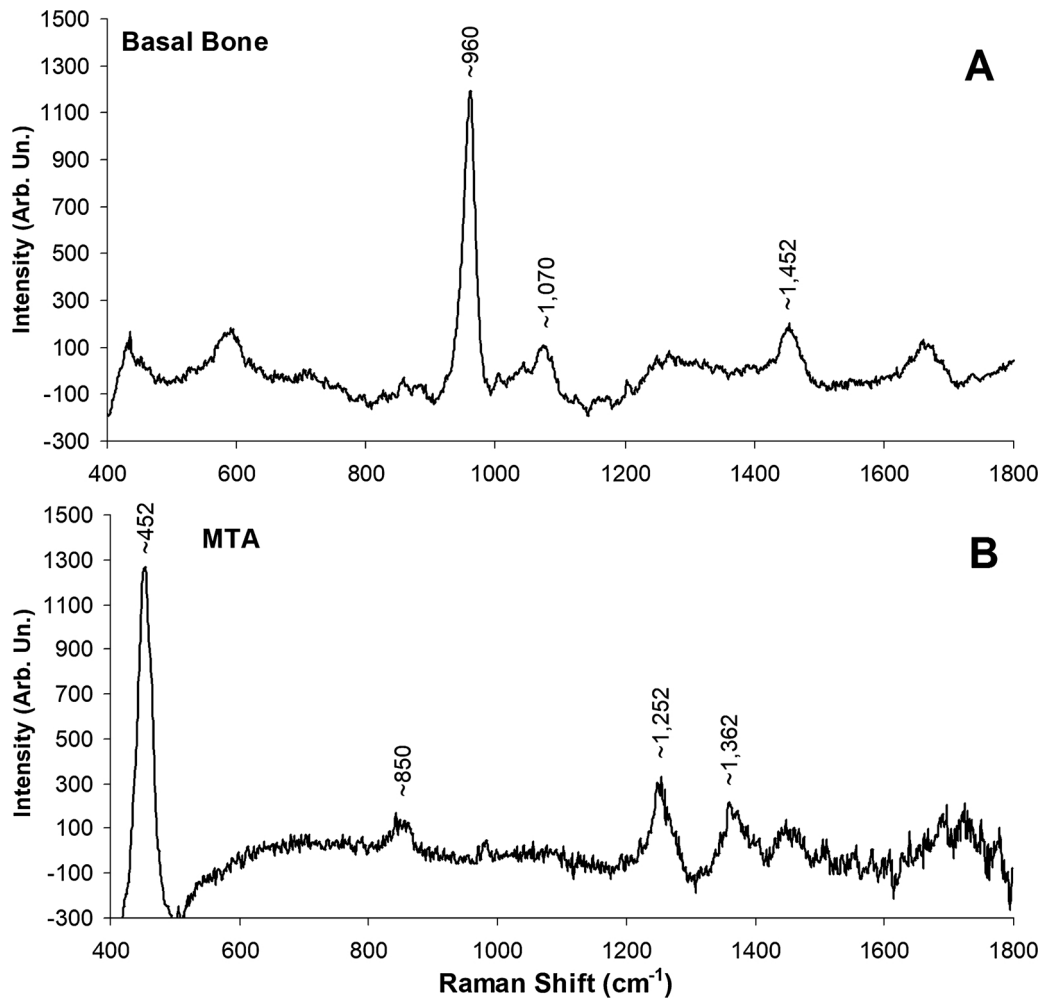


Fig. 2. A) Raman spectrum of untreated (basal) bone showing the presence of characteristic peak at  $\sim 960\text{ cm}^{-1}$  assigned to phosphate hydroxyapatite and used as a marker of the degree of bone mineralization. B) MTA spectrum showing the absence of the peak at  $\sim 960\text{ cm}^{-1}$  and the presence of an intense peak in the region of  $\sim 452\text{ cm}^{-1}$ , which was used as a marker of MTA presence in bone tissue treated with the biomaterial.

(4 points of  $5.1 \text{ J/cm}^2$ ) per session, 300 s,  $142.8 \text{ J/cm}^2$  per treatment] or LED [Fisioled®, MM Optics Ltda., São Carlos, SP, Brazil,  $\lambda = 850 \pm 10 \text{ nm}$ , 150 mW, spot area =  $0.5 \text{ cm}^2$ ,  $20.4 \text{ J/cm}^2$  (4 points of  $5.1 \text{ J/cm}^2$ ) per session, 64 s,  $142.8 \text{ J/cm}^2$  per treatment]. Prior the laser or LED irradiation, the optical power was checked (Optical Power Meter PM30, Thorlabs Instrumentation Inc., Newton, NJ, USA). The irradiation started immediately after treatment prior the suturing and it was repeated at every other day for 2 weeks, transcutaneously. After suturing (Trusynth® 4-0 polyglactin and Trusynth® 4-0 nylon, Sutures India Pvt Ltd. Bangalore, Karnataka, India), the animals received intramuscular antibiotics (penicillin, streptomycin, Pentabiótico® 20.000 UI, 0.2 mL/kg IM; Lab. Forte Dogde Saúde Animal Ltda., Campinas, SP, Brazil, and flunixin meglumine, Banamine® 10 mg/mL, 0.1 mL/kg IM, MSD Saúde Animal Ltda., Cruzeiro, SP, Brazil).

Following animal death 30 days after fracture, the bone samples were withdrawn and longitudinally cut under refrigeration (Isomet TM1000, Buehler Illinois Tool Works Inc., Markham, ON, Canada) (Fig. 1B) and stored in liquid nitrogen without fixation.

#### 2.4. Raman spectroscopy

At the time of Raman study, the samples were warmed to room temperature and a drop of saline was used during spectroscopic measurements to keep moist and avoid tissue burn. Raman spectra were collected at the bone fracture surface (Fig. 1B) by means of a dispersive near-infrared Raman spectrometer composed of a diode laser (785 nm, 100 mW power output, B&W Tek Inc., Newark, DE, USA), imaging spectrograph (model Shamrock™ spectrograph SR-303I-A, Andor Technology Ltd., Belfast, North Ireland) and CCD camera (back-illuminated, deep-depletion camera, model iDus™ DU401A-BR-DD, Andor Technology Ltd., Belfast, North Ireland), resulting in spectra from 600 to  $1,800 \text{ cm}^{-1}$  with resolution of about  $6 \text{ cm}^{-1}$ . The spectrometer is connected to a microcomputer with software which controls integration time and number of acquisitions. The spectrometer is coupled to a fiber-optic Raman probe (model BAC-100-785, B&W Tek Inc., Newark, DE, USA) for the tissue excitation and Raman scattering collection, providing repeatable excitation-collection geometry. The spectrograph had the wavenumber and intensity calibration verified prior the data collection by collecting the spectrum of naphthalene (wavenumber) and tungsten lamp (intensity) and compared to stored standard spectra.

Raman spectra were collected via the probe at the defect site with integration time set to 20 s in five points, resulting in 15 spectra per group (90 spectra in the dataset). A Raman spectrum of non-treated bone and a spectrum of MTA cement were also produced and acted as control (Fig. 2). Spectra were collected at the same day to avoid changes in laser power and experimental setup.

The spectra from bone defects were pre-processed to remove cosmic ray spikes and fluorescence background. Cosmic rays were removed manually and the fluorescence was removed by using the mpoly routine with 5<sup>th</sup> order polynomial [46], facilitating the visualization of the peaks found on the bone. This background removal routine was implemented in Matlab® 5.1 software (The Mathworks Inc., Newark, NJ, USA).

#### 2.5. Data analysis

The intensities of the peaks of interest ( $\sim 960$ ,  $1,070$  and  $\sim 1,452 \text{ cm}^{-1}$ ) were tabulated as these intensities can be related to the concentration of phosphate HA, carbonated HA and protein (mainly collagen), respectively, on the bone. One-way ANOVA was applied to these intensities to verify significant differences between the groups in each peak of interest. First, normality of the distribution was tested [Kolmogorov-Smirnov (KS) test, where  $p > 0.10$  was considered normal distribution] and depending on the results of the KS test, Tukey (parametric) or Dunn (non-parametric) *post-hoc* test was employed ( $p$ -value  $< 0.05$  to reject the null hypothesis and be considered

significant).

Since several variables are evaluated at the same time (type of graft and use of phototherapy) during the time course, it has been conducted a two-way ANOVA with balanced design. The ANOVA general linear model (GLM) was used to verify if these variables influenced the outcome of the bone repair based on the intensity of Raman peaks of interest, since the intensities of these peaks are related to the differences in the constitution of bone tissue [47]. In this model, the effect of treatments on bone repair during the experimental time was evaluated depending on the predictor variables: the use of grafts (None or MTA) and the irradiation (None, Laser or LED), which were transformed into a “dummy variable”. Statistical analyses were conducted with  $p$ -value  $< 0.05$  to reject the null hypothesis and models’ adequacy was evaluated with the adjusted  $R^2$ . Statistical analysis was performed using Minitab® 15.0 software (Minitab Inc., Belo Horizonte, MG, Brazil).

### 3. Results

The spectral characterization of the untreated (basal) bone and the biomaterial used (MTA) are presented in Fig. 2. The untreated (basal) bone spectrum presents peak of phosphate hydroxyapatite at  $\sim 960 \text{ cm}^{-1}$  (Fig. 2A) was used as a marker of bone repair in view that it represents the major component of mineralized bone. The MTA spectrum (Fig. 2B) presents a strong peak at  $\sim 452 \text{ cm}^{-1}$  and less intense peaks at  $\sim 850$ ,  $\sim 1,250$  and  $\sim 1,360 \text{ cm}^{-1}$ . Since phosphate is the major component of mineralized bone HA, the peak at  $\sim 960 \text{ cm}^{-1}$  was used as a marker of bone repair (Fig. 2A). The peak of MTA at  $\sim 452 \text{ cm}^{-1}$  is the most characteristic one and was used as marker of its presence in bone fractures (Fig. 2B).

The spectral characterization of the fractured bone treated with IRF (miniplates) revealed important spectral change when the biomaterial MTA was used. In these groups (Fig. 3), it was noticed the presence of an intense peak in the region of  $\sim 452 \text{ cm}^{-1}$ , which is assigned to MTA. Also, it is noted a strong spectral noise in these samples, which resemble the spectral pattern of the MTA (shot noise from MTA fluorescence due to the laser excitation).

The intensities of the peaks of phosphate HA ( $\sim 960 \text{ cm}^{-1}$ ), carbonated HA ( $\sim 1,070 \text{ cm}^{-1}$ ) and bone matrix (collagen,  $\sim 1,452 \text{ cm}^{-1}$ ) were obtained at 30<sup>th</sup> day for all groups and the mean intensities are plotted in Fig. 4. Note that the groups graft and irradiated with laser showed higher intensities for all three peaks. One-way ANOVA showed that the intensities of the three peaks presented statistically significant differences comparing all groups (Dunn multiple comparison test,  $p < 0.0001$ ). Table 2 summarizes the statistical results of the ANOVA comparing selected groups (Dunn’s multiple comparison tests). On regards the presence of the peak phosphate HA in the spectra of bone tissues (Fig. 4A), the group IRF grafted with MTA and irradiated with laser showed significantly higher intensity when compared to the groups irradiated with LED and non-irradiated. On regards the presence of carbonated HA (Fig. 4B) and collagen (Fig. 4C), the behavior was similar to the one observed for the phosphate HA, being significantly higher intensity for both compounds observed on the group grafted and irradiated with laser compared to the LED and non-irradiated. Interesting to observe that the group grafted with MTA and the group irradiated with laser presented significantly higher intensity of carbonate HA compared to the group IRF, while not presenting changes in the peaks of phosphate HA and collagen.

The ANOVA GLM evaluated the significance of the intensities of the peaks from Fig. 4 and the results are seen in Table 3. The statistical results showed that either the use of irradiation (laser or LED) or grafting with MTA significantly influenced the intensity of all peaks.

### 4. DISCUSSION

Despite the enormous potential for recovery, the regeneration of bone tissue may fail due to several local and/or systemic factors,

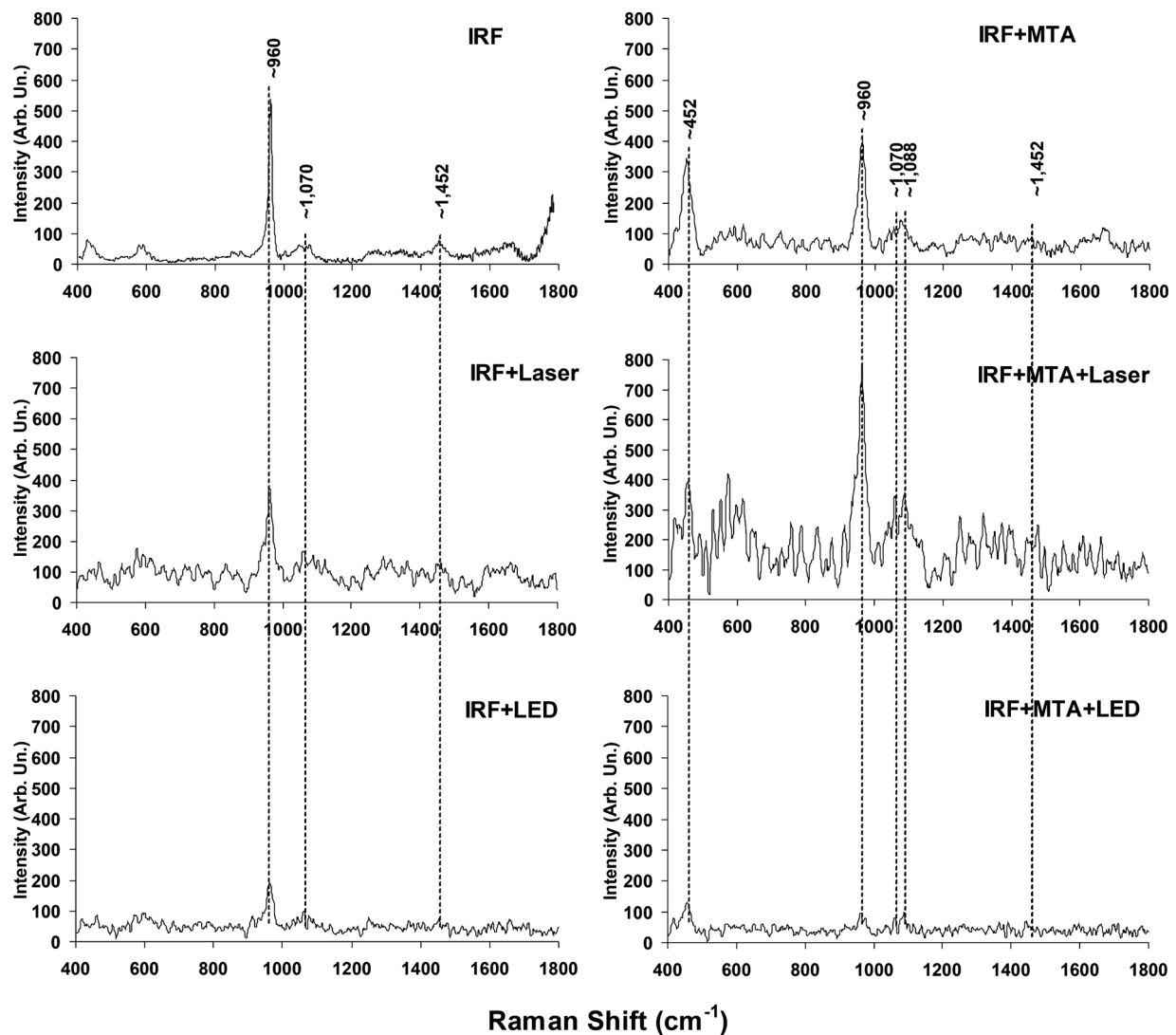


**Fig. 3.** Mean spectra of the groups of bone fractures with IRF miniplate treated or not with laser/LED and MTA. The presence of the characteristic peak at  $\sim 960 \text{ cm}^{-1}$  in bone is attributed to phosphate HA. In the groups in which MTA was used, the spectral characteristics of the biomaterial were also present as the peak at  $\sim 452 \text{ cm}^{-1}$ , the pattern (intensity and bandwidth) of the phosphate HA peak at  $\sim 960 \text{ cm}^{-1}$  also changed, and the peak of carbonated HA at  $\sim 1,070 \text{ cm}^{-1}$  shifted to  $\sim 1,088 \text{ cm}^{-1}$  (hydroxyapatite-like calcium carbonate).

including bone losses. Therefore, it is necessary to use bone grafts, mainly the autologous, to stimulate bone formation, as well as stabilization techniques of the bone stumps and thus achieve proper repair. Modern surgery uses several grafts to replace bone losses. Therefore, finding ways to improve the outcome of the bone repair must be a goal. Nowadays, the discussion remains about how to obtain an adequate recovery, which type of biomaterial would be ideal to be used as a graft in replacing the autogenous graft, and which type of technique is most appropriate for each case [1,4,5,14–20,32,46–48].

Complete fractures with or without bone loss need to be fixed and immobilized to stabilize the bone fragments. Up to now, the two techniques mainly used are internal rigid fixation (IRF using miniplates and titanium screws, or semi-rigid internal fixation using stainless steel wire (wire osteosynthesis - WO). In this study, IRF was used as this system due to its reported benefits over WO for the treatment of fractures of the maxillofacial complex [4,14,15,49].

The MTA was chosen as a graft due to its biocompatibility, non-toxicity, antibacterial properties, increased tissue dissolution and induction of bone formation. Previous histological studies showed that a new bone is formed adjacent to the MTA when it is brought into contact with artificial bone defects [21–31]. Despite MTA being widely studied,

no other study associating it with laser or LED phototherapy in the repair of bone fractures was reported.

There is convincing evidence in the recent literature that phototherapies show positive effects in bone repair after fractures [4,5,14–16,41] without causing any harm or adverse effects. The light-bone interaction explains the stimulatory effects on the bone including faster removal of necrotic tissue, increase of collagen and DNA synthesis, increase of  $\text{Ca}^{+}$  deposition, increase of periosteum cells function and osteoblast and osteocyte function, improved neovascularization, stimulus in endochondral ossification, earlier differentiation of mesenchymal cells, increase of preosteogenic cells with stimulus of callus formation [4,5,14–16,41]. Effect of stimulus in the bone formation was found when light was associated to autologous bone grafts, allografts and guided bone regeneration (GBR) [50].

The protocol of phototherapy used in our study is like many previous reported ones in which it was demonstrated that the use of phototherapies causes important tissue responses during the repair of different bone defects by quickening the repair process as well as improving in the quality of the newly formed bone [1,4,5,14–20,32,47–49,51]. The protocol used in this study started immediately after the surgical procedure and was repeated at every

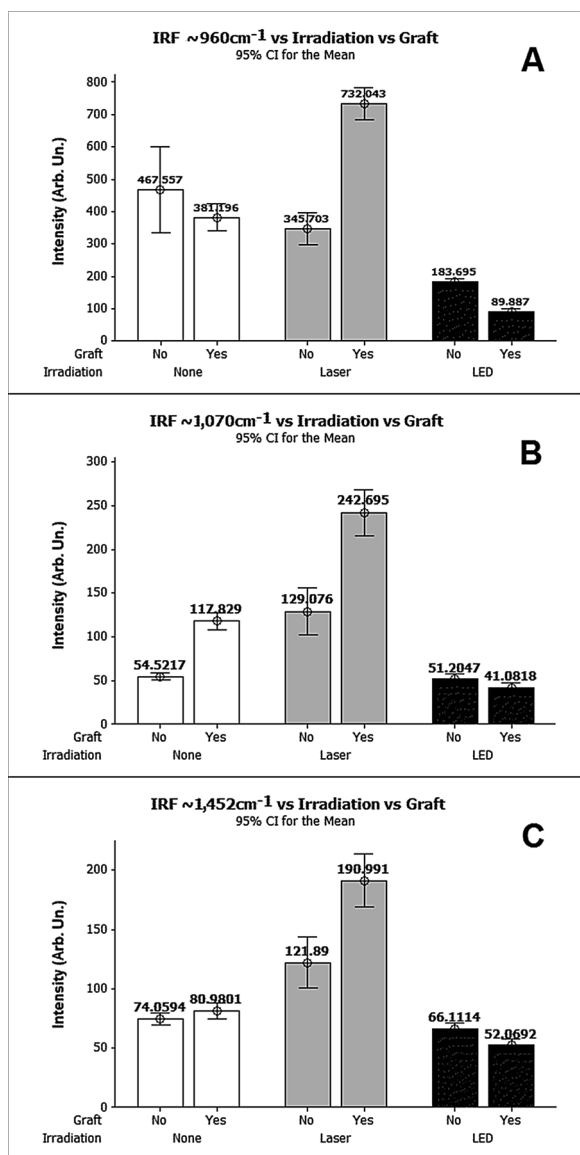


Fig. 4. Mean intensities of the peaks of: A) phosphate hydroxyapatite (~960 cm<sup>-1</sup>); B) carbonated hydroxyapatite (~1,070 cm<sup>-1</sup>); and C) collagen from matrix (~1,452 cm<sup>-1</sup>) observed on the experimental groups of IRF miniplate grafted or not with MTA and plotted according to the type of irradiation.

other day for 15 days because the cellular component (mainly fibroblasts and osteoblasts) is more prominent and more likely to be affected by light at early stages as well as the recruitment of inflammatory cells during the first 36-h post-surgery [52]. Therefore, the observational period used was 30 days postoperative, where the repair process is in a more advanced stage (the initial phase of cellular proliferation occurring up to 15<sup>th</sup> day), and could be influenced after the initial stimulus provided by the phototherapies. This period is, being widely used to evaluate the bone repair in several studies already published [1,4,5,14–20,32,47–49,51].

It has been observed a strong fluorescence background on the Raman spectra when MTA was used causing a lower signal-to-noise ratio. The presence of remnants of MTA was seen as a strong peak at ~452 cm<sup>-1</sup> (Fig. 3). Regarding the presence of this peak in such spectra, this corroborates the histological results that show the permanence of the MTA in the fracture area at the end of the experimental period (unpublished data). The group IRF + MTA + LED presented the lower intensity, suggesting a less advance of the repair with this light source as all the peaks of interest presented lower intensity considering the

Table 2

Summary of the one-way ANOVA applied to the intensities of the selected Raman peaks.

| Comparison                            | p value (Dunn's multiple comparison) |                        |                        |
|---------------------------------------|--------------------------------------|------------------------|------------------------|
|                                       | 960 cm <sup>-1</sup>                 | 1,070 cm <sup>-1</sup> | 1,452 cm <sup>-1</sup> |
| IRF vs. IRF + MTA                     | NS                                   | < 0.001                | NS                     |
| IRF vs. IRF + Laser                   | NS                                   | < 0.01                 | NS                     |
| IRF vs. IRF + LED                     | < 0.01                               | NS                     | NS                     |
| IRF vs. IRF + MTA + Laser             | < 0.001                              | < 0.001                | < 0.001                |
| IRF vs. IRF + MTA + LED               | < 0.001                              | NS                     | < 0.01                 |
| IRF + MTA vs. IRF + Laser             | NS                                   | NS                     | NS                     |
| IRF + MTA vs. IRF + LED               | < 0.001                              | < 0.001                | NS                     |
| IRF + MTA vs. IRF + MTA + Laser       | < 0.001                              | < 0.001                | < 0.001                |
| IRF + MTA vs. IRF + MTA + LED         | < 0.001                              | < 0.001                | < 0.001                |
| IRF + Laser vs. IRF + LED             | < 0.01                               | < 0.001                | < 0.05                 |
| IRF + Laser vs. IRF + MTA + Laser     | < 0.001                              | < 0.001                | < 0.001                |
| IRF + Laser vs. IRF + MTA + LED       | < 0.001                              | < 0.001                | < 0.001                |
| IRF + LED vs. IRF + MTA + Laser       | < 0.001                              | < 0.001                | < 0.001                |
| IRF + LED vs. IRF + MTA + LED         | < 0.001                              | NS                     | NS                     |
| IRF + MTA + Laser vs. IRF + MTA + LED | < 0.001                              | < 0.001                | < 0.001                |

NS – not significant

Table 3

Summary of the ANOVA GLM applied to the intensities of the selected Raman peaks.

| Raman Peak              | Variable      | Adjusted SS | F      | p value |
|-------------------------|---------------|-------------|--------|---------|
| ~960 cm <sup>-1</sup>   | Graft*        | 810704      | 13.80  | < 0.001 |
|                         | Irradiation** | 9688861     | 82.47  | < 0.001 |
| ~1,070 cm <sup>-1</sup> | Graft*        | 331331      | 55.40  | < 0.001 |
|                         | Irradiation** | 1282072     | 107.19 | < 0.001 |
| ~1,452 cm <sup>-1</sup> | Graft*        | 54882       | 54882  | < 0.001 |
|                         | Irradiation** | 693471      | 88.16  | < 0.001 |

\* None or MTA

\*\* None, Laser or LED

time interval of 30 days (Fig. 3). As the repair effect is both wavelength and dose dependent, the interaction of the LED light with the graft biomaterial was not as expected and therefore more studies need to be addressed to identify the dose/wavelength dependency to promote advanced bone repair.

The evaluation of the bone fracture repair in the groups was based on the spectral pattern of phosphate HA peak (~960 cm<sup>-1</sup>) as one of the markers of bone repair considering that it represents a major component in the mineralized bone and is absent in the spectrum of the MTA. The spectral pattern of fractured tissue treated with IRF was similar for the two groups with respect to the ~960 cm<sup>-1</sup> peak. However, the spectral pattern changed when the biomaterial MTA was used [53].

It has been found significant changes in the intensities of the peaks of phosphate HA (~960 cm<sup>-1</sup>), carbonated HA (~1,070 cm<sup>-1</sup>) and proteins (collagen, ~1,452 cm<sup>-1</sup>) (Fig. 4) between irradiated and non-irradiated fractures. It has been observed higher intensities of the peak of phosphate HA (Fig. 4A) for the groups irradiated with laser when compared to LED and non-irradiated groups. Also, there was significant difference between the two irradiated groups, being the group grafted and irradiated with laser the one showing higher peak intensity. This result corroborates previous reports demonstrating that the use of laser irradiation increases the deposition of phosphate HA using different models of bone lesions and grafting, including on fractures [1,4,5,14–16,41,47,49,51]. It is interesting to observe that LED irradiation did not promote increase in the phosphate HA; instead, the intensity was lower even than the group not irradiated.

On regards the presence of the carbonated HA, an agreement was found with regard the phosphate HA, being the intensities of the ~1,070 cm<sup>-1</sup> peak on the laser irradiated and grafted group higher compared to the other groups (Fig. 4B). Interestingly the carbonated HA

increased for the group grafted with MTA and not irradiated. As the carbonated HA is a transitional form of apatite that is replaced by the phosphate form in more advanced stages of the repair, it is considered a marker of bone mineralization [1,4,5,14–16,20,32,47–49,51]. In the laser irradiated groups, both phosphate and carbonated HA were highly increased. The LED irradiation, in contrast, presented a reduced intensity of the carbonated HA as occurred with the phosphate HA, suggesting a reduction in bone formation or a delay in the repair process.

The deposition of collagen during the repair of the fractured bone (peak  $\sim 1,452\text{ cm}^{-1}$ ) can be seen by its higher intensity on the laser irradiated groups; as occurred with the peaks of phosphate and carbonated HA, the highest intensity was found on the group grafted and irradiated with laser (Fig. 4C). Collagen is an important component for a successful repair of any biological tissue since it serves as a meshwork for deposition of hydroxyapatite and subsequent mineralization of the bone [1,4,5,14–16,20,32,47–49,51]. As occurred with the intensities of the HA peaks, the groups irradiated with LED presented intensity of collagen lower than the non-irradiated groups.

The statistical analysis showed that the levels of phosphate HA, carbonated HA and collagen were influenced by both the irradiation (either laser or LED) or grafting (MTA), thus being significant for the outcome of bone repair. Bone maturation, as marked by the peak of  $\sim 960\text{ cm}^{-1}$ , was more pronounced in the group FIR + MTA + Laser. The results of the intensities of phosphate and carbonated HA peaks (Fig. 4A and B) confirm this finding. As collagen (marked by the peak of  $\sim 1,452\text{ cm}^{-1}$ ) is the precursor of a meshwork for mineralization, increased collagen content may be indicative of a more pronounced bone formation (Fig. 3).

An interesting finding was the fact that the peak of the carbonated HA at  $1,070\text{ cm}^{-1}$  was shifted to the region of  $\sim 1,088\text{ cm}^{-1}$  in the groups treated with MTA (IRF + MTA, IRF + MTA + Laser and IRF + MTA + LED). This shift may be attributed to the presence of calcium carbonate ( $\text{CaCO}_3$ ), with peak at around  $\sim 1,090\text{ cm}^{-1}$ . As MTA is rich in calcium (silicate, sulphate and aluminate), it releases the cationic content, being calcium the highest proportion, and induces the production of calcium carbonate ( $\text{CaCO}_3$ ), a hydroxyapatite-like substance with high osteogenic potential [52]. Therefore MTA can create an intermediate step that induces the formation of a scaffold of  $\text{CaCO}_3$  for the deposition of bone tissue. This calcium-rich biomaterial increases the bone repair by boosting the phosphate HA formation leading to an increase in the mineral content over the matrix.

It is known that in the region of  $\sim 1,077\text{ cm}^{-1}$  is observed a peak for phosphate HA [ $\nu_3$  asymmetric stretching of phosphate apatite ( $\text{PO}_4^{3-}$ ), which may contribute to the intensity of the carbonated HA peak at  $\sim 1,070\text{ cm}^{-1}$ . The carbonated HA is a transitory form of HA observed during bone repair; the presence of this peak for the MTA groups could be indicative of higher level of mineralization at these sites filled with MTA; however, this aspect should be evaluated in a future study.

Improved bone maturation on irradiated subjects is due to increased deposition of calcium hydroxyapatite (CHA) as, during initial stages of repair, the osteoblastic activity is chiefly proliferative, and deposition starts later, this results in the formation of immature bone, still poor in CHA [50]. This later maturation represents the improved ability of more mature osteoblasts to secrete CHA in irradiated subjects. The observed differences in the rate of deposition of CHA between irradiated and control subjects is probably due to the choice of a wavelength with higher penetration and the ability to increase changes at cellular levels, such as improved ATP synthesis, early osteoblastic differentiation and the release of growth factors. The cellular reactions such as ATP synthesis promotion, electron transport chain stimulation, and cellular pH reduction, and these biochemical and cell membrane changes may increase activities of macrophage, fibroblast, lymphocyte and the other healing cells [50,54].

The results of the present study corroborate with previous studies by our group showing that the use of Raman spectroscopy is efficacious on

assessing bone repair on several models including on fractures [4,5,14–16]. Researchers have been proposing methods for assessing the bone quality in rat tibiae *in vivo* and noninvasively by Raman spectroscopy with fiber optic probes [55], which may provide new possibilities for following the evolution of the repair *in situ*.

## 5. CONCLUSION

The results of the present experimental study indicated that the use of the MTA associated with laser phototherapy improved the repair process of complete fractures in tibia treated with IRF, by evaluating the intensities of the Raman peaks of phosphate HA ( $\sim 960\text{ cm}^{-1}$ ), carbonated HA ( $1,070\text{ cm}^{-1}$ ) and collagen matrix ( $\sim 1,452\text{ cm}^{-1}$ ). The laser irradiation increased the deposition of phosphate and carbonated HA and also collagen in the MTA-filled defects. Also, the results suggested that the MTA induced the formation of a scaffold of calcium carbonate for the bone tissue deposition. However, the presence of the peak of the biomaterial MTA over a long period in the MTA-filled groups suggests a delay in the process of scaffold promoted by the MTA, without affecting significantly the results of bone repair.

## Compliance with Ethical Standards

The authors of the present investigation state that they have no competing conflict of interest to declare. Author (Blinded 8) received Productivity Fellowship and author (Blinded 1) received Grant, both from the Brazilian National Council for Scientific and Technological Development (CNPq) (No. 305680/2014-5 and No. 470630/2012-4, respectively). The study has been approved by The Animal Ethics Committee of the School of Dentistry of the Federal University of Bahia (Protocol 17/10/2012), respecting the statement on welfare of animals used in research approved by the Brazilian government.

## Acknowledgements

L. Silveira Jr. acknowledges National Council for Scientific and Technological Development (CNPq) for the Productivity Fellowship (Grant no. 305680/2014-5). This work was supported by the National Council for Scientific and Technological Development (CNPq) (Grant no. 470630/2012-4).

## References

- [1] A.L.B. Pinheiro, M.E.M.M. Gerbi, Photoengineering of Bone Repair Processes, *Photomed Laser Surg* 24 (2) (2006) 169–178, <https://doi.org/10.1089/pho.2006.24.169>.
- [2] B. Wopenka, J.D. Pasteris, A mineralogical perspective on the apatite in bone, *Mater Sci Eng* 25 (2) (2005) 131–143, <https://doi.org/10.1016/j.msec.2005.01.008>.
- [3] L. Claes, B. Willie, The enhancement of bone regeneration by ultrasound, *Progr Biophys Mol Biol* 93 (1–3) (2007) 384–398, <https://doi.org/10.1016/j.pbiomolbio.2006.07.021>.
- [4] A.L.B. Pinheiro, N.R.S. Santos, P.C. Oliveira, G.T.S. Aciole, T.A. Ramos, T.A. Gonzalez, L. Silveira, The efficacy of the use of IR laser phototherapy associated to biphasic ceramic graft and guided bone regeneration on surgical fractures treated with miniplates: a Raman spectral study on rabbits, *Lasers Med Sci* 28 (2) (2012) 513–518, <https://doi.org/10.1007/s10103-012-1096-1>.
- [5] A.L.B. Pinheiro, N.R.S. Santos, P.C. Oliveira, G.T.S. Aciole, T.A. Ramos, T.A. Gonzalez, L. Silveira, The efficacy of the use of IR laser phototherapy associated to biphasic ceramic graft and guided bone regeneration on surgical fractures treated with wire osteosynthesis: a comparative laser fluorescence and Raman spectral study on rabbits, *Lasers Med Sci* 28 (3) (2012) 815–822, <https://doi.org/10.1007/s10103-012-1166-4>.
- [6] X. Liu, R. Lyon, H.T. Meier, J. Thometz, S.T. Haworth, Effect of Lower-Level Laser Therapy on Rabbit Tibial Fracture, *Photomed Laser Surg* 25 (6) (2007) 487–494, <https://doi.org/10.1089/pho.2006.2075>.
- [7] M.F. Al-Habib, M.O. Salman, F.W. Faleh, I.M. Al-Ani, Histological observation related to the use of laser and ultrasound on bone fracture healing, *Int Med J Malaysia* 10 (2) (2011) 29–35 <https://journals.iium.edu.my/imjm/index.php/eimj/article/download/66/64>.
- [8] K. Kawasaki, N. Shimizu, Effects of low-energy laser irradiation on bone remodeling during experimental tooth movement in rats, *Lasers Surg Med* 26 (3) (2000) 282–291, [https://doi.org/10.1002/\(sici\)1096-9101\(2000\)26:3<282::aid-lsm6>3.0.co;2-x](https://doi.org/10.1002/(sici)1096-9101(2000)26:3<282::aid-lsm6>3.0.co;2-x).
- [9] E. Fávoro-Pípi, S.M. Feitosa, D.A. Ribeiro, P. Bossini, P. Oliveira, N.A. Parizotto,

- A.C.M. Renno, Comparative study of the effects of low-intensity pulsed ultrasound and low-level laser therapy on bone defects in tibias of rats, *Lasers Med Sci* 25 (5) (2010) 727–732, <https://doi.org/10.1007/s10103-010-0772-2>.
- [10] S. Kazem Shakouri, J. Soleimanpour, Y. Salekzamani, M.R. Oskuae, Effect of low-level laser therapy on the fracture healing process, *Lasers Med Sci* 25 (1) (2009) 73–77, <https://doi.org/10.1007/s10103-009-0670-7>.
- [11] M. Khadra, N. Kasem, H.R. Haanaes, J.E. Ellingsen, S.P. Lyngstadaas, Enhancement of bone formation in rat calvarial bone defects using low-level laser therapy, *Oral Surg Oral Med Oral Pathol Oral Radiol Endod* 97 (6) (2004) 693–700, <https://doi.org/10.1016/j.tripleo.2003.11.008>.
- [12] A. Renno, P.A. McDonnell, N.A. Parizotto, E.L. Laakso, The effects of laser irradiation on osteoblast and osteosarcoma cell proliferation and differentiation in vitro, *Photomed Laser Surg* 25 (4) (2007) 275–280, <https://doi.org/10.1089/pho.2007.2055>.
- [13] A. Stein, D. Benayahu, L. Maltz, U. Oron, Low-level laser irradiation promotes proliferation and differentiation of human osteoblasts in vitro, *Photomed Laser Surg* 23 (2) (2005) 161–166, <https://doi.org/10.1089/pho.2005.23.16>.
- [14] C.B. Lopes, M.T. Pacheco, L. Silveira Jr, M.C. Cangussú, A.L. Pinheiro, The effect of the association of near infrared laser therapy, bone morphogenetic proteins, and guided bone regeneration on tibial fractures treated with internal rigid fixation: A Raman spectroscopic study, *J Biomed Mater Res A* 94 (4) (2010) 1257–1263, <https://doi.org/10.1002/jbm.a.32800>.
- [15] A.L. Pinheiro, C.B. Lopes, M.T. Pacheco, A. Brugnera Jr, F.A. Zanin, M.C. Cangussú, L. Silveira, Raman spectroscopy validation of DIAGNodent-assisted fluorescence readings on tibial fractures treated with laser phototherapy, BMPs, guided bone regeneration, and miniplates, *Photomed Laser Surg* 28 (Suppl. 2) (2010) S89–S97, <https://doi.org/10.1089/pho.2009.2674>.
- [16] C.B. Lopes, M.T. Pacheco, L. Silveira Jr, J. Duarte, M.C. Cangussú, A.L. Pinheiro, The effect of the association of NIR laser therapy BMPs, and guided bone regeneration on tibial fractures treated with wire osteosynthesis: Raman spectroscopy study, *J Photochem Photobiol B* 89 (2–3) (2007) 125–130, <https://doi.org/10.1016/j.jphotobiol.2007.09.011>.
- [17] A.L.B. Pinheiro, A.P. Soares, L.G.P. Soares, F.B. Carvalho, A.M.C. Marques, Phototherapies Usage for Improving Bone Repair: From the Bench to the Dental Chair, *Lasers Med Sci* 32 (8) (2017) 1682, <https://doi.org/10.1590/S0103-64402003000300007>.
- [18] C.S. Torres, J.N. dos Santos, J.S. Monteiro, P.G. Amorim, A.L. Pinheiro, Does the use of laser photobiomodulation, bone morphogenetic proteins, and guided bone regeneration improve the outcome of autologous bone grafts? An in vivo study in a rodent model, *Photomed Laser Surg* 26 (4) (2008) 371–377, <https://doi.org/10.1089/pho.2007.2172>.
- [19] J.B. Weber, A.L. Pinheiro, M.G. de Oliveira, F.A. Oliveira, L.M. Ramalho, Laser therapy improves healing of bone defects submitted to autologous bone graft, *Photomed Laser Surg* 24 (1) (2006) 38–44, <https://doi.org/10.1089/pho.2006.24.38>.
- [20] L.G. Soares, E.B. Magalhães, C.A. Magalhães, C.F. Ferreira, A.M. Marques, A.L. Pinheiro, New bone formation around implants inserted on autologous and xenografts irradiated or not with IR laser light: A histomorphometric study in rabbits, *Braz Dent J* 24 (3) (2013) 218–223, <https://doi.org/10.1590/0103-6440201302186>.
- [21] M. Parirokh, M. Torabinejad, Mineral trioxide aggregate: A comprehensive literature review - Part I: chemical, physical, and antibacterial properties, *J Endod* 36 (1) (2010) 16–27, <https://doi.org/10.1016/j.joen.2009.09.006>.
- [22] M. Torabinejad, C.U. Hong, S.J. Lee, M. Monsef, T.R. Pitt Ford, Investigation of mineral trioxide aggregate for root end filling in dogs, *J Endod* 21 (12) (1995) 603–608, [https://doi.org/10.1016/S0099-2399\(06\)81112-X](https://doi.org/10.1016/S0099-2399(06)81112-X).
- [23] M. Torabinejad, C.U. Hong, T.R. Pitt Ford, Physical and chemical properties of a new root end filling material, *J Endod* 21 (7) (1995) 349–353, [https://doi.org/10.1016/S0099-2399\(06\)80967-2](https://doi.org/10.1016/S0099-2399(06)80967-2).
- [24] M. Torabinejad, C.U. Hong, T.R. Pitt Ford, S.P. Kaiyawasam, Tissue reaction to implanted super-EBA and mineral trioxide aggregate in the mandible of guinea pigs: a preliminary report, *J Endod* 21 (11) (1995) 569–571, [https://doi.org/10.1016/S0099-2399\(06\)80987-8](https://doi.org/10.1016/S0099-2399(06)80987-8).
- [25] M. Torabinejad, N. Chivian, Clinical applications of mineral trioxide aggregate, *J Endod* 25 (3) (1999) 197–205, [https://doi.org/10.1016/S0099-2399\(99\)80142-3](https://doi.org/10.1016/S0099-2399(99)80142-3).
- [26] E. Al-Rabeah, H. Perinpanayagam, D. MacFarland, Human alveolar bone cells interact with ProRoot and tooth-colored MTA, *J Endod* 32 (9) (2006) 872–875, <https://doi.org/10.1016/j.joen.2006.03.019>.
- [27] J.D. Regan, J.L. Gutmann, D.E. Witherspoon, Comparison of Diaket and MTA when used as root-end filling materials to support regeneration of the periradicular tissues, *Int Endod J* 35 (10) (2002) 840–847, <https://doi.org/10.1046/j.1365-2591.2002.00582.x>.
- [28] T.R. Moretton, C.E. Brown Jr, J.J. Legan, A.H. Kafrawy, Tissue reactions after subcutaneous and intraosseous implantation of mineral trioxide aggregate and ethoxybenzoic acid cement, *J Biomed Mater Res* 52 (3) (2000) 528–533, [https://doi.org/10.1002/1097-4636\(20001205\)52:3<528::aid-jbm11>3.0.co;2-9](https://doi.org/10.1002/1097-4636(20001205)52:3<528::aid-jbm11>3.0.co;2-9).
- [29] A. Bystrom, R. Claesson, G. Sundqvist, The antibacterial effect of camphorated paramonochlorophenol, camphorated phenol and calciumhydroxide in the treatment of infected root canals, *Endod Dent Traumatol* 1 (5) (1985) 170–175, <https://doi.org/10.1111/j.1600-9657.1985.tb00652.x>.
- [30] P.J. Mitchell, T.R. Pitt Ford, M. Torabinejad, F. McDonald, Osteoblast biocompatibility of mineral trioxide aggregate, *Biomaterials* 20 (2) (1999) 167–173, [https://doi.org/10.1016/S0142-9612\(98\)00157-4](https://doi.org/10.1016/S0142-9612(98)00157-4).
- [31] P. Taddei, A. Tinti, M.G. Gandolfi, P.L. Rossi, C. Prati, Vibrational study on the bioactivity of Portland cement-based materials for endodontic use, *J Mol Struct* 924–926 (2009) 548–554, <https://doi.org/10.1016/j.molstruc.2008.11.002>.
- [32] A.L. Pinheiro, G.T. Aciole, M.C. Cangussú, M.T. Pacheco, L. Silveira, Effects of laser phototherapy on bone defects grafted with mineral trioxide aggregate, bone morphogenetic proteins, and guided bone regeneration: A Raman spectroscopic study, *J Biomed Mater Res A* 95 (4) (2010) 1041–1047, <https://doi.org/10.1002/jbm.a.32930>.
- [33] J. Camilleri, Hydration mechanisms of mineral trioxide aggregate, *Int Endod J* 40 (6) (2007) 462–470, <https://doi.org/10.1111/j.1365-2591.2007.01248.x>.
- [34] L. Tronstad, J.O. Andreasen, G. Hasselgren, L. Kristerson, I. Riis, pH changes in dental tissues after root canal filling with calcium hydroxide, *J Endod* 7 (1) (1981) 17–21, [https://doi.org/10.1016/S0099-2399\(81\)80262-2](https://doi.org/10.1016/S0099-2399(81)80262-2).
- [35] E.B. Hanlon, R. Manoharan, T.W. Koo, K.E. Shafer, J.T. Motz, M. Fitzmaurice, J.R. Kramer, I. Itzkan, R.R. Dasari, M.S. Feld, Prospects for in vivo Raman spectroscopy, *Phys Med Biol* 45 (2) (2000) R1–R59, <https://doi.org/10.1088/0031-9155/45/2/201>.
- [36] L.M. Moreira, L. Silveira, F.V. Santos, J.P. Lyon, R. Rocha, R.A. Zângaro, A.B. Villaverde, M.T.T. Pacheco, Raman spectroscopy: A powerful technique for biochemical analysis and diagnosis, *Spectroscopy* 22 (1) (2008) 1–19.
- [37] C. Krafft, B. Dietzek, M. Schmitt, J. Popp, Raman and coherent anti-Stokes Raman scattering microspectroscopy for biomedical applications, *J Biomed Opt* 17 (4) (2012) 040801, <https://doi.org/10.3233/SPE-2008-0326>.
- [38] I. Pence, A. Mahadevan-Jansen, Clinical instrumentation and applications of Raman spectroscopy, *Chem Soc Rev* 45 (7) (2016) 1958–1979, <https://doi.org/10.1039/c5cs00581g>.
- [39] M.D. Morris, G.S. Mandair, Raman assessment of bone quality, *Clin Orthop Relat Res* 469 (8) (2011) 2160–2169.
- [40] A. Carden, M.D. Morris, Application of vibrational spectroscopy to the study of mineralized tissues (review), *J Biomed Opt* 5 (3) (2000) 259–268.
- [41] A.L.B. Pinheiro, L.G.P. Soares, A.C.P. Silva, N.R.S. Santos, A.P.L.T. Silva, B.L.R.C. Neves, A.P. Soares, L. Silveira, Laser/LED phototherapy on the repair of tibial fracture treated with wire osteosynthesis evaluated by Raman spectroscopy, *Lasers Med Sci* 33 (8) (2011) 1657–1666, <https://doi.org/10.1007/s10103-018-2508-7>.
- [42] O. Heinisch, W.G. Cochran, Sampling Techniques, 2<sup>nd</sup> edn., John Wiley & Sons, New York, 1963.
- [43] S.C.P.S. Oliveira, J.S.C. Monteiro, G.M. Pires-Santos, F.J.P. Sampaio, A.P. Soares, L.G.P. Soares, A.L.B. Pinheiro, LED antimicrobial photodynamic therapy with phenothiazinium dye against *Staphylococcus aureus*: An in vitro study, *J Photochem Photobiol B* 175 (2017) 46–50, <https://doi.org/10.1016/j.jphotobiol.2017.08.029>.
- [44] F.B. Carvalho, A.S. Andrade, A.F.S. Barbosa, M.C. Aguiar, M.C.T. Cangussú, A.L.B. Pinheiro, L.M.P. Ramalho, Evaluation of laser phototherapy ( $\lambda$  780 nm) after dental replantation in rats, *Dent Traumatol* 32 (6) (2016) 488–494, <https://doi.org/10.1111/edt.12289>.
- [45] J.A. Reis, J.N. dos Santos, B.S. Barreto, P.N. de Assis, P.F. Almeida, A.L.B. Pinheiro, Photodynamic Antimicrobial Chemotherapy (PACT) in osteomyelitis induced by *Staphylococcus aureus*: Microbiological and histological Study, *J Photochem Photobiol B* 149 (2016) 235–242, <https://doi.org/10.1016/j.jphotobiol.2015.06.005>.
- [46] C.A. Lieber, A. Mahadevan-Jansen, Automated method for subtraction of fluorescence from biological Raman spectra, *Appl Spectrosc* 57 (11) (2003) 1363–1367, <https://doi.org/10.1366/00037020322554518>.
- [47] L.G. Soares, A.M. Marques, J.M. Aciole, M.G. da Guarda, M.C. Cangussú, L. Silveira, A.L. Pinheiro, Do laser/LED phototherapies influence the outcome of the repair of surgical bone defects grafted with biphasic synthetic microgranular HA +  $\beta$ -tricalcium phosphate? A Raman spectroscopy study, *Lasers Med Sci* 29 (5) (2014) 1575–1584, <https://doi.org/10.1007/s10103-014-1563-y>.
- [48] A.L. Pinheiro, L.G. Soares, A.M. Marques, M.C. Cangussú, M.T. Pacheco, L. Silveira, Biochemical changes on the repair of surgical bone defects grafted with biphasic synthetic micro-granular HA +  $\beta$ -tricalcium phosphate induced by laser and LED phototherapies and assessed by Raman spectroscopy, *Lasers Med Sci* 32 (3) (2017) 663–672, <https://doi.org/10.1007/s10103-017-2165-2>.
- [49] J.M.S. Aciole, G.T.S. Aciole, L.G.P. Soares, A.F.S. Barbosa, J. Santos, Bone repair on fractures treated with osteosynthesis, IR laser, bone graft and guided bone regeneration: histomorphometric study, *AIP Conf Proc* 1364 (1) (2017) 60–65, <https://doi.org/10.1063/1.3626913>.
- [50] A.L.B. Pinheiro, A.M.C. Marques, L.G.P. Soares, A.F.S. Barbosa, Bone Biomodulation, in: P.M. Freitas, A. Simões (Eds.), *Lasers in Dentistry: Guide for Clinical Practice*, Wiley-Blackwell, São Paulo, 2015, pp. 196–206.
- [51] A.L. Pinheiro, L.G. Soares, A.M. Marques, J.M. Aciole, R.A. de Souza, L. Silveira, Raman ratios on the repair of grafted surgical bone defects irradiated or not with laser ( $\lambda$ 780 nm) or LED ( $\lambda$ 850 nm), *J Photochem Photobiol B* 138 (2014) 146–154, <https://doi.org/10.1016/j.jphotobiol.2014.05.022>.
- [52] K.R. Fernandes, D.A. Ribeiro, N.C. Rodrigues, C. Tim, A.A. Santos, N.A. Parizotto, H.S. de Araujo, P. Driusso, A.C. Rennó, Effects of low-level laser therapy on the expression of osteogenic genes related in the initial stages of bone defects in rats, *J Biomed Opt* 18 (3) (2013) 038002, <https://doi.org/10.1117/1.JBO.18.3.038002>.
- [53] M.G. Gandolfi, K. Van Landuyt, P. Taddei, E. Modena, B. Van Meerbeek, C. Prati, Environmental scanning electron microscopy connected with energy dispersive X-ray analysis and Raman techniques to study ProRoot mineral trioxide aggregate and calcium silicate cements in wet conditions and in real time, *J Endod* 36 (5) (2010) 851–857, <https://doi.org/10.1016/j.joen.2009.12.007>.
- [54] L.F. Freitas, M.R. Hamblin, Proposed mechanisms of photobiomodulation or low-level light therapy, *IEEE J Sel Top Quantum Electron* 22 (3) (2016) 7000417, <https://doi.org/10.1109/JSTQE.2016.2561201>.
- [55] P.I. Okagbare, D. Begun, M. Tecklenburg, A. Awonusi, S.A. Goldstein, M.D. Morris, Noninvasive Raman spectroscopy of rat tibiae: approach to in vivo assessment of bone quality, *J Biomed Opt* 17 (9) (2012) 090502, <https://doi.org/10.1089/ten.tec.2013.0622>.